X-ray Spectroscopy of the Iron Site in Soybean Lipoxygenase-1: Changes in Coordination upon Oxidation or Addition of Methanol†

Robert C. Scarrow,*,‡ Milton G. Trimitsis,‡ Charles P. Buck,‡ Geoffrey N. Grove,‡ Rebecca A. Cowling,§ and Mark J. Nelson*,§

Department of Chemistry, Haverford College, Haverford, Pennsylvania 19041, and Central Research and Development, E. I. du Pont de Nemours & Co., Wilmington, Delaware 19880-0328

Received August 30, 1994; Revised Manuscript Received October 14, 1994⊗

ABSTRACT: Iron K-edge X-ray spectroscopy (XANES and EXAFS) was used to study iron coordination in frozen solutions of soybean lipoxygenase-1 (SLO). The intensity of the 1s→3d pre-edge transition of native iron(II) lipoxygenase is greater than what was found for six-coordinate high-spin iron(II) model complexes, but comparable to that of a five-coordinate model. This and a relatively short average bond length determined by EXAFS (2.13 Å) indicate that the native lipoxygenase in our frozen samples is five-coordinate, excluding possible bonds longer than 2.5 Å. The coordination of the iron(II) in native lipoxygenase changes when methanol (as low as 0.1%) or glycerol (20%) is added to the buffer prior to freezing. The addition of methanol diminishes the pre-edge transition and increases EXAFS-derived bond lengths by 0.04 Å, indicating a change to six-coordination. The small pre-edge feature in active iron(III) lipoxygenase suggests six-coordination. EXAFS indicates a short, 1.88 Å Fe−O bond, which, given other spectroscopic and crystallographic evidence, is assigned to coordinated hydroxide. The average of the remaining bond lengths is 2.11 Å. The iron coordination in iron(III) lipoxygenase is less affected by the presence of alcohols than is the site in the iron(II) enzyme. Bond valence sums indicate that the bond lengths for lipoxygenase derived from our EXAFS analyses are comparable to those of crystallographically characterized model complexes. The flexibility of the coordination number in SLO^N (native SLO) and the presence of an $[Fe^{III}OH]^{2+}$ unit in SLO^A (active SLO) are of possible mechanistic importance.

Soybean lipoxygenase-1 is a non-heme iron enzyme that catalyzes the oxygenation of polyunsaturated fatty acids (Gardner, 1991; Siedow, 1991). For example, it catalyzes the reaction of linoleic acid with dioxygen to produce 13-HPOD.[1] The observation of alkyl and peroxyl fatty acid radicals generated by lipoxygenase under a variety of conditions (Chamulitrat & Mason, 1989; Nelson & Cowling, 1990; Nelson et al., 1990, 1994) supports a mechanism in which the active-site ferric ion oxidizes the 1,4-diene of linoleic acid to a fatty acid radical that reacts with dioxygen, ultimately yielding the hydroperoxide (Figure 1) (de Groot et al., 1975). An alternate mechanism proposes that the role of the ferric ion is to facilitate deprotonation of the substrate by coordinating the resulting carbanion, yielding an organometallic intermediate that reacts with dioxygen (Corey & Nagata, 1987). Characterization of the structure and reactivity of the iron ion in lipoxygenase is key to understanding the mechanism of dioxygenation.

Spectroscopic and magnetic measurements have been used to explore the coordination environment of the iron ion. Native (as isolated) soybean lipoxygenase (SLO^N) contains a single ferrous ion. Oxidation to Fe^{3+} produces the active enzyme (SLO^A). Magnetic susceptibility measurements established that the iron is high-spin in both SLO^N and SLO^A (Cheesbrough & Axelrod, 1983; Slappendel et al., 1982c). CD and variable-temperature MCD spectroscopy of ferrous (Whittaker & Solomon, 1986, 1988) and ferric (Zhang et al., 1991) lipoxygenases supports distorted octahedral coordination in both. At least one of the iron ligands in ferric lipoxygenase is water or hydroxide, as determined by the observation of line-broadening in the EPR spectra of samples prepared using $H_2{}^{17}O$ (Nelson, 1988b). Visible spectroscopy (Cox et al., 1988) of catechol complexes of ferric lipoxygenase suggests that three of the native ligands to the iron are neutral, presumably histidines. The large number of neutral ligands leads to a relatively high reduction potential for the iron in SLO^A (ca. 0.6 V vs NHE) (Nelson, 1988a), lending credence to the ability of the enzyme to oxidize its substrates to fatty acid radicals.

† X-ray data were collected at the National Synchrotron Light Source, Brookhaven National Laboratory, which is supported by the U.S. Department of Energy, Divisions of Materials Science and Chemical Science (DOE contract no. DE-AC02-76CH00016). Research at Haverford College was supported by American Chemical Society Petroleum Research Fund Grant No. 21967-GB3, NIH Grant GM51045-01, and the Undergraduate Biological Sciences Education Initiative of the Howard Hughes Medical Institute. This is Contribution No. 6624 from DuPont Central Research and Development.

* Authors to whom correspondence should be addressed.

‡ Haverford College.

§ Du Pont.

⊗ Abstract published in *Advance ACS Abstracts,* November 15, 1994.

[1] Abbreviations: acac, acetylacetonate anion; Bis-Tris, 2-bis[(2-hydroxyethyl)amino]-2-(hydroxymethyl)-1,3-propanediol; BVS, bond valence sum; CD, circular dichroism spectroscopy; DMF, *N,N*-dimethylformamide; EPR, electron paramagnetic resonance; esd, estimated standard deviation of n determinations ($=[\Sigma(y - y_{av})^2/(n - 1)]^{1/2}$); EXAFS, extended X-ray absorption fine structure; gof, goodness of fit; $HB(3,5\text{-}i\text{-}Pr_2pz)_3$, tris(3,5-diisopropylpyrazol-1-yl)borate anion; 13-HPOD, 13(*S*)-hydroperoxy-9,11(*E,Z*)-octadecadienoic acid; MCD, magnetic CD; *N*-MeIm, *N*-methylimidazole; NMR, nuclear magnetic resonance; *o*-phen, 1,10-phenanthroline; SLO, soybean lipoxygenase-1 (SLO^N, native; SLO^A, active); TIEOH, 1,1,2-tris(*N*-methylimidazol-2-yl)ethanol; XANES, X-ray absorption near-edge spectroscopy.

0006-2960/94/0433-15023$04.50/0

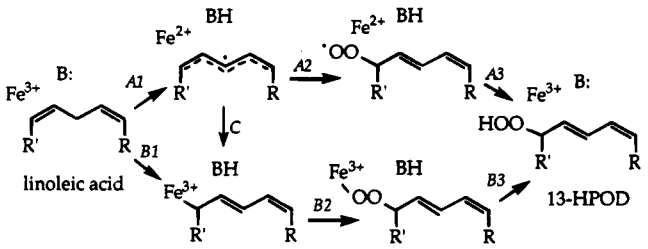

FIGURE 1: Proposed lipoxygenase mechanisms (R = $(CH_2)_7COOH$, R′ = $(CH_2)_4CH_3$): pathway A, radical mechanism (de Groot et al., 1975); pathway B, organometallic mechanism (Corey & Nagata, 1987). A hybrid mechanism involving steps A1, C, B2, and B3 is proposed in the Discussion.

A previous X-ray absorption study concluded that the ferrous ion in SLO^N is six-coordinate, on the basis of both the quality of the fits to the EXAFS and the small size of the Fe 1s→3d pre-edge transition in the XANES. Analysis of the EXAFS data using multiple scattering theory led to a model with four imidazoles at 2.12−2.14 Å and two oxygen ligands at 1.93−1.99 Å (Feiters et al., 1990; Navaratnam et al., 1988). We note that these results are highly unusual for high-spin iron(II). The reported average bond length of ca. 2.07 Å is about 0.1 Å shorter than that found in crystal structures of high-spin Fe(II) complexes with four nitrogen- and two oxygen-donor ligands: r_{av} = 2.16 Å in diaquabis-(5-methyl-1,2,4-triazolo[1,5-*a*]pyrimidine-N^3)bis(thiocyanato-*N*)iron(II) (Cingi et al., 1986) and r_{av} = 2.20 Å in $Fe^{II}(HB(3,5\text{-}i\text{-}Pr_2pz)_3)(OBz)(CH_3CN)$ (Kitajima et al., 1990).

Analogous studies of SLO^A also indicated an octahedral metal ion, but with three imidazole ligands at 2.10−2.11 Å and three oxygen ligands at 1.90−1.91 Å; this was interpreted as supporting ligand exchange upon oxidation of the iron (Van der Heijdt et al., 1992). The average metal−ligand bond length reported for SLO^A was 2.00 Å, which is 0.04−0.07 Å shorter than those found in crystal structures of high-spin iron(III) complexes with three nitrogen- and three oxygen-donor ligands: r_{avg} = 2.04 Å for (2-(benzimidazol-2-ylmethyl)phenolato)(2-oxo-3-methylbenzenato)bis(*N*-methylimidazole)iron(III) (McDevitt et al., 1990), 2.06 Å for (3,5-di-*tert*-butylcatecholato-*O*,*O*′-((bis(2-pyridylmethyl)-amine)acetato-*O*)iron(III) (Cox & Que, 1988), and 2.06 Å for $[(HBpz_3)Fe^{III}]_2(\mu\text{-}O)(\mu\text{-}OAc)_2$ (Armstrong et al., 1984). Thus, the bond distances reported in these studies indicate either a novel, highly compressed six-coordinate iron center in both SLO^N and SLO^A or an error in the determination of the bond lengths or the overall coordination number.

Two recent 2.6 Å resolution X-ray crystallographic structures of lipoxygenase show four (Boyington et al., 1993) or five (Minor et al., 1993) ligands to the iron, respectively. Both structures indicate coordination by histidines 499, 504, and 690 and monodentate coordination by the C-terminal carboxylate of isoleucine 839; additional coordination by asparagine 694 was found by Minor et al. (1993). Both of these coordination models are at odds with spectroscopic results that indicate six-coordinate iron in both SLO^N and SLO^A (Feiters et al., 1990; Navaratnam et al., 1988; Van der Heijdt et al., 1992; Whittaker & Solomon, 1986, 1988; Zhang et al., 1991). However, more recently, Minor et al. have refined their structure to higher resolution and found electron density indicating water as a sixth ligand to the iron (B. Axelrod, personal communication).

In view of the uncertainty about the coordination number and bond lengths of the iron center in the native and active forms of lipoxygenase, we have reexamined the EXAFS and XANES of SLO^N and SLO^A. We also have studied the effects of pH, reduction by substrate, and the presence of low molecular weight alcohols on the active-site iron ion. Our studies allow us to hypothesize structures for the active-site iron that rationalize all of the spectroscopic data and that are consistent with the highest resolution crystal structure currently available.

This paper summarizes our results from X-ray spectroscopy as they pertain to the first coordination sphere of the iron in lipoxygenase. A subsequent paper will describe the multiple scattering analysis of the high-frequency components of the lipoxygenase EXAFS, from which information pertaining to the number and geometry of coordinated histidine groups is obtained.

EXPERIMENTAL SECTION

Sample Preparation. Soybean lipoxygenase was purified and assayed according to published procedures (Nelson, 1988a). Samples used had specific activities in excess of 220 units/mg and iron content in excess of 0.9 moles per mole of enzyme. SLO^A was prepared by addition of purified 13-HPOD to SLO^N until the first appearance of absorbance at 585 nm indicated the oxidation was complete. Enzyme samples were dialyzed vs two changes of 1000 vol of 0.1 M Bis-Tris/acetate (pH 5.8) (25 °C), 0.1 M Bis-Tris/acetate (pH 6.8) (25 °C), or 0.05 M sodium borate/acetate (pH 9.0) (25 °C) to achieve pH 6, 7, or 9, respectively, at 4 °C. Each sample was concentrated to between 2 and 3 mM protein using an Amicon Centricon concentrator, transferred to an aluminum sample holder (2 × 20 mm slot, 1 mm thick, 1 mil Mylar coverslips), and frozen and stored in liquid nitrogen. Methanol, ethanol, pyrocatechol, or linoleic acid was added immediately before the solutions were loaded into the sample holders. Prior to the addition of pyrocatechol or linoleate, enzyme samples were left under argon in serum vials for at least 30 min, and the solutions were subsequently transferred via a gas-tight syringe to sample holders that had recently been flushed with argon.

Solid samples were ground with boron nitride as a diluant and packed into sample holders with only one Mylar coverslip, and 0.4 mil Kaptan electrical tape was used to provide the other window.

Data Collection. X-ray spectroscopy was performed at three beam lines of the National Synchrotron Light Source at Brookhaven National Laboratory (Table 1). Between two gas ionization detectors (with outputs i_0 and i_1), sample holders were mounted in the evacuated chamber of a liquid nitrogen cryostat (Janis). (Samples from run I were maintained at ca. 30 K by the Displex refrigeration unit of beam line X-9a.)

Between the second and third gas ionization detectors was a sample of powdered $(Et_4N)(FeCl_4)$ suspended in Duco cement; its sharp pre-edge transition at 7113.0 eV was used for energy calibration (Scarrow et al., 1987). The fluorescence detector (i_F) was placed perpendicular to the X-ray beam to measure the 2p→1s X-ray fluorescence of the sample. For experimental runs A, B, and G, a large solid angle gas ionization detector was used with a Mn filter and Sollar slits to reduce scattered light. For other runs a 13-

Table 1: Meanings of the Three- or Four-Character Sample Codes Used in This Paper

character 1:	sample origin	character 3:	conditions
2	prepared from SLO^N	1	BN pellet, ca. 80 K
3	prepared from SLO^A	2	BN pellet, ca. 300 K
a	$Fe^{II}(acac)_3$	6	frozen, pH 5.8
b	$Fe^{II}(N\text{-MeIm})_6(BF_4)_2$	7	frozen, pH 6.8
c	$Fe^{II}(ox)(H_2O)_2$	9	frozen, pH 9.0
d	$Fe^{II}(H_2O)_6(BF_4)_2$	character 4:	additives
e	$Fe^{II}(o\text{-phen})_3(ClO_4)_2$	c	pyrocatechol, 5 mM
character 2:	beam line and monochromator used	e	0.1% (v/v) EtOH
		g	20% (v/v) glycerol
A, E, I	X9a, Si 111	m	0.1% (v/v) MeOH
C, F	X9a, Si 220	M	1% (v/v) MeOH
B	X11a, Si 111	s	3 mM linoleic acid and 0.1% MeOH
D, G	X19a, Si 220		

element Ge solid state detector (Canberra) was positioned so that the total count rate for each channel was generally below 30 000 s^{-1}.[2] Energy discriminators were used to isolate the Fe Kα fluorescence (6.4 keV) from the higher energy scattered X-rays.

Data Analysis. Data were analyzed on Macintosh computers using *Igor* (WaveMetrics, Lake Oswego, OR) for data averaging and graphing and *SSExafs* (available by request from R.C.S.) for least-squares fitting of parametrized equations describing the XANES and EXAFS.

The edge-normalized XANES (ξ_{obs}) and EXAFS (χ_{obs}; defined above the edge only) were obtained by dividing the raw data by edge height ($\Delta\mu$), predicted K-edge absorption fall-off (μ_{rel}^{FeK}) (McMaster et al., 1969), and a detector efficiency factor (F_{rel}) (see Table S1):[3]

$$\xi_{obs} = \chi_{obs} + 1 = \frac{\text{average}(i_F/i_0)}{F_{rel}(E)\,\mu_{rel}^{FeK}(E)\Delta\mu} + \text{baseline} \quad (1)$$

Transmission data from model complexes were treated similarly, except that $\ln(i_0/i_1)$ replaces i_F/i_0 in eq 1, and $F_{rel} = 1$ throughout the energy range.

For least-squares fits, the residual minimized and reported is the goodness of fit (gof):

$$\text{gof} = \sqrt{\frac{n_{FT}}{n_{FT} - n_{var}} \frac{\sum \omega_Y^2 [Y_{obs} - Y_{calcd}]^2}{n_{obs}}} \quad (2)$$

where Y is the data fit (ξ or $k^3\chi$), ω_Y is the weight given to each of the n_{obs} data, n_{var} is the number of variables refined, and n_{FT} is the number of real and imaginary values contributing to the back-transform for Fourier-filtered data; $n_{FT} = n_{obs}$ for unfiltered data.

XANES Fits. In the initial data fitting, *SSExafs* fit ξ_{obs} by refining the height ($\Delta\mu$), position, and width of the edge jump, the coefficients of the cubic-spline baseline (discontinuous second and third derivatives at 7125, 7405, and 7645 eV), and n, r, and σ^2 for the first coordination sphere. The data fit were the pre-edge baseline (6900−7103 eV, $\omega_Y = 10$; 7103−7107 eV, $\omega_Y = 100$), the rising edge above the 1s→3d peak (E_1 to $E_1 + 4$ eV, $\omega_Y = 100$), and the EXAFS from $k = 3$ to 14.3 $Å^{-1}$ ($\omega_Y = k^3$ $Å^3$). $E_1 \approx 7115$ eV was chosen to give good fits (see table captions). The area of the 1s→3d peak, A_{pre}, was calculated by the integration of $\xi_{obs} - \xi_{calc}$ in the $\omega_Y = 0$ region between 7107 eV and E_1. The photoelectron wavenumber, k, is calculated using $E_0 = 7125$ eV in eq 3:

$$k = [(2m_e/\hbar)(E - E_0)]^{1/2} \quad (3)$$

Fourier Filtering. The EXAFS were Fourier-filtered to isolate contributions from first coordination sphere scatterers. The $k^3\chi$ was interpolated to a 0.056 $Å^{-1}$ grid between $k = 1.01$ and 14.28 $Å^{-1}$, multiplied by a 5% window function (Scarrow et al., 1987), and back-transformed between $r' = 1.0$ and 2.3 Å to obtain the Fourier-filtered spectrum. During least-squares fitting, the same transformations were applied to the calculated $k^3\chi$.

Empirical Weighting. An experimental error estimate (ee) for Fourier-filtered $k^3\chi$ was constructed on the basis of the estimated standard deviation (esd) for the EXAFS of protein samples deemed to have the same iron environment (based on sample history and initial analyses of EXAFS and XANES). The ee used for first sphere Fourier-filtered spectra was a linear interpolation of the following (k ($Å^{-1}$), ee ($Å^{-3}$)) pairs: (2.2, 0.14), (4, 0.19), (8, 0.26), (10, 0.42), (13, 0.88), (14.3, 0.56). The Fourier-filtered EXAFS $k^3\chi$ was fit between $k = 2.2$ and 14.3 $Å^{-1}$, and the gof was calculated using $\omega_Y = 1/\text{ee}$.

EXAFS Amplitude (f) and Phase (α) Functions. The program FEFF 5.05 (Rehr et al., 1991, 1992) was used to calculate f and α, as well as the dependence of f and α on the absorber−scatterer distance (r). Details are given in the caption to Table S2, which lists the calculated functions.

RESULTS

Samples Examined. We have determined the iron K-edge EXAFS and XANES spectra of frozen samples of lipoxygenase prepared in various buffers and various oxidation states. EXAFS samples and data sets are identified by codes of three or four characters (Table 1).

The spectra of SLO^N at pH 7 and 9 are superimposable, and spectra of SLO^A show no changes between pH 6 and 9. Because of the higher oxidation state of iron in SLO^A, its pre-edge peak (at 7113 eV) occurs about 1.5 eV higher than the pre-edge peak in SLO^N, with an even greater shift of up to 3 eV occurring in the most steeply rising part of the edge (Figure 2a). Differences are also apparent in the EXAFS region.

The addition of either 0.1% (20 mM) or 1% methanol to solutions of SLO^N resulted in a third distinct spectrum. In contrast, the addition of methanol or ethanol to SLO^A changed the spectrum only slightly (Figure 3). Addition of 20% glycerol to SLO^N or SLO^A resulted in spectral changes similar to those caused by the addition of methanol.

We also obtained EXAFS spectra for samples of SLO^A in which the iron was chemically reduced to Fe^{2+} under an O_2-free atmosphere by the addition of either pyrocatechol or

[2] Data set 3I7M had total count rates as high as 40 000 s^{-1} on some detectors. We experimentally determined a 3 μs detector dead time under the conditions employed (shaping time = 0.25 μs). Correction of this data set (using $F = F_{obs}(t + Ct_d)/t$, where t is time, C is the total counts, and t_d is the dead time) resulted in a 3% *relative* decrease in both A_{pre} and n. This is much less than the uncertainties in these parameters, so we have not corrected other data sets where the total count rate was less than 30 000 s^{-1}.

[3] Tables S1−S9 are supplementary material; see statement at end of paper.

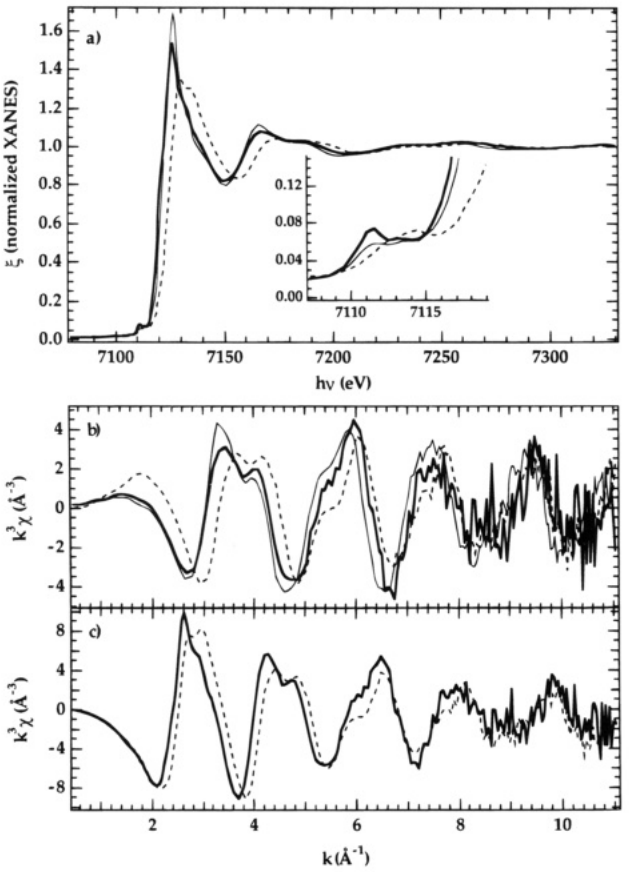

FIGURE 2: (a) Normalized and baseline-corrected X-ray spectra for samples of SLO^N (thick solid line, 2F9), SLO^N·MeOH (thin solid line, 2D7m) and SLO^A (dashed line, 3D9) at pH 9. Inset: XANES, ξ_{obs}, in the 1s→3d peak region. (b) EXAFS spectra ($k^3\chi$), where k is calculated using $E_0 = 7125$ eV, as used in the remainder of this paper. (c) $k^3\chi$ calculated using $E_0 = 7100$ eV (SLO^N) or 7102 eV (SLO^A) to approximate the spectra of Van der Heijdt et al. (1992) (see Discussion).

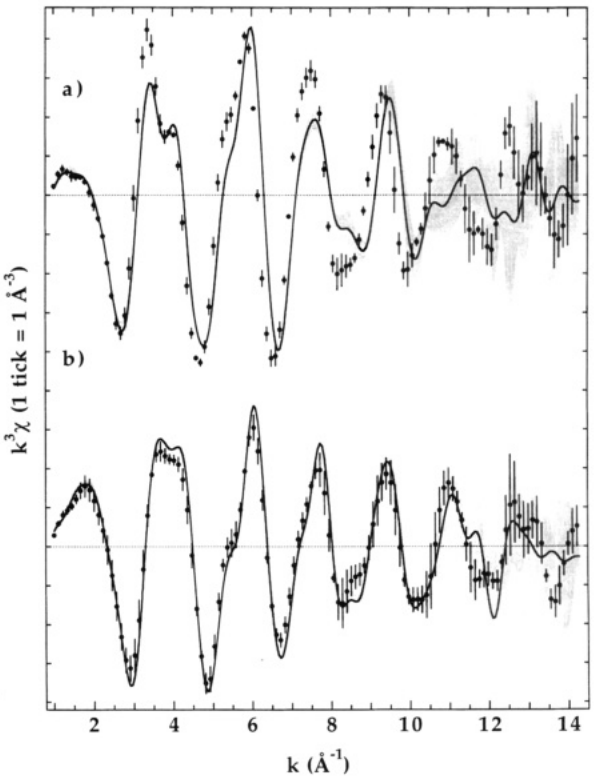

FIGURE 3: Fourier-smoothed EXAFS of (a) SLO^N and (b) SLO^A samples without (solid line, shaded) or with (dots, error bars) added alcohol. The shading and error bars indicate the ± esd ranges from averaging data sets with similar spectra: SLO^N—2E9, 2F9, 2D7, and 2A7; SLO^N·MeOH—2E7m, 2D7m, and 2I9M; SLO^A—3D9, 3D7, 3A7, 3B7, and 3F6; SLO^A+alcohol—3D9e, 3F7m, 3I9M, and 3I9g.

sodium linoleate in the minute before the samples were frozen (samples 3D7c, 3D7s, and 3E9s).

XANES Analysis. The intensity of the 1s→3d pre-edge peak is enhanced by mixing between the 3d and 4p orbitals that becomes more important with increasing distortion of the iron site away from centrosymmetry. Consequently, the pre-edge peak area, A_{pre}, may be used as a marker for coordination number; this has been demonstrated in detail for high-spin ferric (Roe et al., 1984) and ferrous (Randall, 1993) complexes.

In order to determine A_{pre}, we subtracted the simulated absorption edge (ξ_{edge}) from ξ_{obs}. Equation 4 models the ξ_{edge} as the integral of a Lorenzian peak ($x_g = 0$), a Gaussian peak ($x_g = 1$), or a combination shape ($0 < x_g < 1$):

$$\xi_{edge} = x_g\left(\mathrm{erf}\left(1.665\frac{E - E_{edge}}{\text{width}}\right)\Big/2\right) + (1 - x_g)\left(\arctan\left(2\frac{E - E_{edge}}{\text{width}}\right)\Big/\pi\right) + 0.5 \quad (4)$$

Because the Lorenzian integral edge shape was used in an earlier extensive study of high-spin ferric complexes (Roe et al., 1984), we initially used eq 4 with $x_g = 0$ to model the edges of the samples of lipoxygenase and model compounds studied in this work (for example, Figure 4a−d). However, when fitting edges of iron(II) samples, we found that by increasing x_g to 0.75, we obtained more convincing fits of the edge, allowing a more accurate determination of A_{pre} (compare Figure 4e to 4d). As shown in Table S3, the A_{pre} values are independent of monochromator resolution for XANES of Fe^{2+} compounds when $x_g = 0.75$ is used, but not when $x_g = 0$ is used.

The magnitude of the 1s→3d peak (A_{pre}) in the XANES of SLO^N indicates that, in frozen solutions of native protein, the Fe^{2+} ion is in an environment of symmetry comparable to that of the five-coordinate model complex Fe^{II}(HB(3,5-*i*-Pr_2pz)$_3$)(OBz) (Kitajima et al., 1990) (compare Figure 4e and 4j). The addition of 0.1% or 1.0% methanol to SLO^N results in a reproducable decrease in the pre-edge peak area of approximately 25% (Figure 4f), indicating that the coordination becomes more centrosymmetric upon the addition of methanol. The observed decrease in A_{pre} of the methanol-treated SLO^N (which we denote SLO^N·MeOH) is mirrorred in the smaller A_{pre} observed (Figure 4j) in the acetonitrile solvate of Fe^{II}(HB(3,5-*i*-Pr_2pz)$_3$)(OBz), which is shown by crystallography to be six-coordinate with bond lengths from 2.05 to 2.30 Å (Kitajima et al., 1990).

The simplest and most obvious explanation for the changes in A_{pre} is that the ferrous ion in frozen solutions of SLO^N is five-coordinate, but can be shifted to six-coordinate in the presence of methanol. However, some caveats must be given on the basis of studies of ferric model complexes (Roe et al., 1984). A seven-coordinate model complex was found to have the same size 1s→3d peak as six-coordinate models; thus, seven-coordination must be considered for SLO^N·MeOH. Furthermore, the presence of the extremely short Fe−oxo

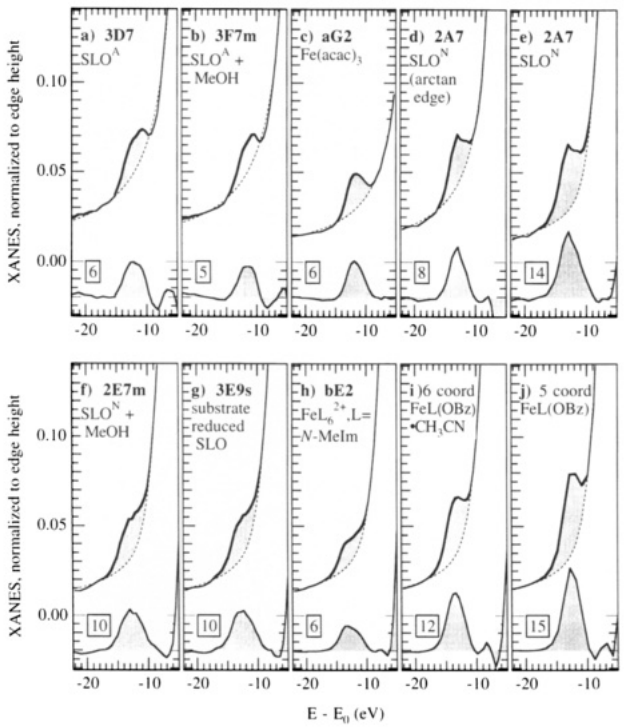

FIGURE 4: Rising edge XANES features of various lipoxygenase samples and model compounds, identified by sample codes (Table 1). Each panel shows the XANES data (ξ_{obs}, upper), the fit to the rising edge using eq 4 (dotted line; panels a−d, $x_g = 0$; panels e−j, $x_g = 0.75$), and the difference representing the isolated pre-edge peak (lower solid line) and its area/electronvolt (boxed). Data for panels i and j (L = HB(3,5-*i*-Pr_2pz)$_3$) were kindly provided prior to publication by Clay Randall and Lawrence Que, Jr.

bond of six-coordinate, oxo-bridged diferric complexes was found to increase the 1s→3d peak area to within the range normally associated with five-coordinate complexes; thus, the five-coordinate-like XANES of SLO^N is also consistent with six-coordination in which one of the bonds is either unusually short or unusually long. If SLO^N were six-coordinate, presumably it would have a greater spread in bond lengths than Fe^{II}(HB(3,5-*i*-Pr_2pz)$_3$)(OBz)(NCCH$_3$); thus, we conclude that SLO^N has only five normal coordination bonds between 2.0 and 2.3 Å and allow for the possibility of a longer or shorter Fe−O or Fe−N bond, on the basis of XANES analysis alone.

The areas of the pre-edge peaks in the spectra of various samples of SLO^A vary from 5 to 9 eV%, which is exactly the range observed in the previous study for six- and seven-coordinate model compounds, and well below the range observed for four- and five-coordinate high-spin mononuclear ferric compounds (Roe et al., 1984). These values, all obtained using $x_g = 0$, are compared in Table S4.

EXAFS Analysis. For the present analysis, we used Fourier filtering to isolate the low-frequency EXAFS due to first coordination sphere atoms (those bound directly to the iron) (Sayers & Bunker, 1988; Scott, 1985). The EXAFS was fit by eq 5 to give information about the type, number (n_i), average distance (r_i), and disorder (σ^2) of atoms in this coordination sphere:

$$\chi_{calcd} = \sum_{i=1}^{\text{no. of shells}} n_i f_i k^{-1} r_i^{-2} \exp(-2(\Delta\sigma^2)k^2) \sin(2kr_i + \alpha_i) \quad (5)$$

The f and α functions (of k and r_i) for Fe−O and Fe−N

Table 2: One-Shell Fits to Fourier-Filtered $k^3\chi$ for Selected Model Complexes[a]

sample	code	n	r (Å)	$\Delta\sigma^2$ (Å^2)	crystallographic r (Å)[b]
Fe(*N*-MeIm)$_6^{2+}$	bE1	5.6	2.200	−0.0008	2.207 (Miller et al., 1989)
	bE2	5.4	2.204	0.0021	2.197, 2.221[c] (Seel et al., 1980)
Fe(phen)$_3^{2+}$	eG1	5.2	1.975	−0.0036	1.969 (Zalkin et al., 1973)
					1.961 (Reiff et al., 1983a)
Fe(acac)$_3$ (X = N)	aG1	7.8	2.011	−0.0014	
Fe(acac)$_3$ (X = O)	aG1	6.4	1.986	−0.0002	1.992 (Iball & Morgan, 1967)
	aG2	6.2	1.986	0.0009	

[a] Except as noted, the scattering atoms are assumed to be nitrogen. Additional details of the refinements are given in Table S5. [b] All distances are for room-temperature crystal structures. [c] Fe(*N*-EtIm)$_6^{2+}$.

Table 3: One-Shell Fits to Fourier-Filtered $k^3\chi$ for Iron(II) Lipoxygenase Samples[a]

samples (codes)	n	r (Å)	$\Delta\sigma^2$ (Å^2)
SLO^N, pH 9 (2E9, 2F9[b])	5.2	2.145	0.0024
SLO^N, pH 7 (2A7, 2D7[b])	5.3	2.141	0.0024
catechol-reduced SLO^A (3D7c)	5.2	2.148	0.0021
SLO^N, 0.1% MeOH (2D7m, 2E7m[b])	6.0	2.185	0.0011
SLO^N, 1.0% MeOH (2I9M)	5.9	2.182	0.0015
SLO^N, 20% glycerol (2I9g)	5.7	2.163	0.0023
linoleate+SLO^A, pH 9 (3E9s)	5.4	2.176	0.0018

[a] Scattering atoms are assumed to be nitrogen. Additional details are found in Table S5. [b] Values shown are averages of refined values for two data sets.

absorber−scatterer pairs were calculated using the program FEFF 5.05 (Rehr et al., 1991, 1992). The mean free path and amplitude reduction terms usually found in the single scattering equation (Sayers & Bunker, 1988; Scott, 1985) were included in the calculated amplitude function, f_i. Also included in f_i were the calculated effects of thermal disorder ($\sigma^2 = 0.004$ Å^2 for Fe−O and 0.005 Å^2 for Fe−N). Thus, $\Delta\sigma^2$ in eq 5 indicates the difference between the actual (static + thermal) disorder and the calculated thermal disorder. Table 2 shows that, for model complexes, eq 5 gives satisfactory determinations of n (within ±15%) and r (within ±0.01 Å), without inclusion of the empirical amplitude reduction factor required by earlier theoretical f and α functions (McKale et al., 1988; Teo & Lee, 1979).

In our initial fits to data from lipoxygenase (Tables 3 and S5), the EXAFS data were modeled by a single shell of n Fe−N bonds at a distance r and disorder $\Delta\sigma^2$. Because f_i and α_i are very similar, Fe−O and Fe−N bonds at similar distances cannot be distinguished by fitting the EXAFS. The Fe(acac)$_3$ data were used to test the effect on n and r of modeling Fe−O as Fe−N: n refined about 25% high, and r refined about 0.02 Å too long. These errors are slightly greater than the accuracy of the EXAFS analyses based on comparisons to crystal structures of model complexes (Table 4, for example); thus, for more accurate average bond lengths for lipoxgyenase, we employed fits with mixed shells of Fe−N and Fe−O bonds constrained to have a common bond length and $\Delta\sigma^2$. For these fits, we used a total of three Fe−N bonds, on the basis of the crystal structures, which each show coordination by three histidine residues.

Table 4: Selected Mixed-Shell and Two-Shell Fits to Fourier-Filtered $k^3\chi$ of SLO^N, SLO^N·MeOH, and $[Fe(N\text{-MeIm})_6]^{2+}$ [a,b]

	fit	shell 1	r (Å)	shell 2	r (Å)	$\Delta\sigma^2$ (Å^2)[c]	Δgof[d] (%)	BVS[e]
SLO^N [f]	1	3N/2O	2.127			0.0030	−7	1.95
	2	3N/3O	2.125			0.0059	+7	*2.31*
	3	2N/3O	2.123	1 N	2.51	0.0034	−20	2.05
SLO^N·MeOH[f]	4	3N/3O	2.164			0.0028	−1	2.08
	5	3N/2O	2.167			0.0005	−2	*1.75*
	6	2N/4O	2.160	1 N	2.541	0.0031	−38	*2.32*
$[Fe(N\text{-MeIm})_6]^{2+}$	7[g]	6N	2.203			0.001	−4	2.05
	8[g]	6N	2.204	1 N	2.56	0.001	−28	2.18
	9[h]	6N	2.210	1 N	2.576	0.0002	−46	*2.29*

[a] Fits 3 and 6 are unreliable because of the similar, but artifactual, 2.5 Å Fe−N distance obtained in fits 8 and 9 to experimental and simulated EXAFS of $[Fe(N\text{-MeIm})_6]^{2+}$. [b] Table S6 gives additional details and fits. [c] $\Delta\sigma^2$ was the same for all shells. [d] Change in gof relative to one-shell fits in which the number of Fe−N bonds is refined (Tables 2 and 3). [e] Bond valence sums outside the range found for high-spin ferrous complexes (1.95−2.24) are italicized. [f] Average of refined values from similar data sets (Figure 3). [g] Average from data sets bE1 and bE2. [h] Fourier-filtered simulated EXAFS calculated by FEFF 5.05 using geometry of imidazole groups found in $[Fe(N\text{-MeIm})_6](BF_4)_2$. The simulated EXAFS includes single and multiple scattering pathways involving all of the atoms of the imidazole ring.

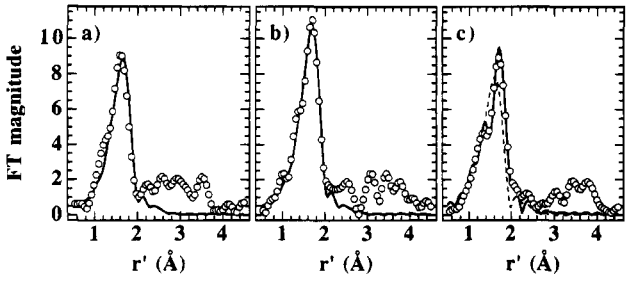

FIGURE 5: EXAFS Fourier transforms for (a) SLO^N, (b) SLO^N·MeOH, and (c) SLO^A. The data (○) are from averages of data sets (see Figure 3). Lines show Fourier transforms of calculated spectra: (a) fit 1, Table 4; (b) fit 4, Table 4; (c) (—) type 3 fit of Table 5, (- - -) type 1 fit of Table 5. Peaks beyond $r' = 2$ Å are due to outer coordination sphere atoms and so are not fit by the first sphere fits shown here.

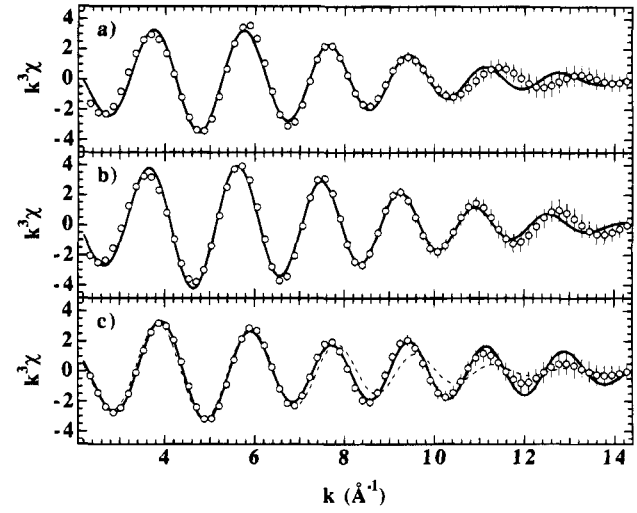

FIGURE 6: Fourier-filtered EXAFS for (a) SLO^N, (b) SLO^N·MeOH, and (c) SLO^A. Data and fits are the same as in Figure 5.

Ferrous Lipoxygenase (Including SLO^N). Single-shell fits to EXAFS of samples of SLO^N in purely aqueous buffers yield $n = 5.2$ nitrogen atoms at $r_{Fe-N} = 2.14$ Å (Table 3). The results are the same for data from samples at pH 7 or 9. The refined n values are expected to be systematically biased to be 10−15% higher than the true value because some of the scatterers are oxygen instead of nitrogen; furthermore, values of n based on EXAFS have errors of up to ±15% in simple model complexes. Thus, the true n for bonds near 2.14 Å is expected to be within +5% to −30% of the refined value, and n from the EXAFS analysis of SLO^N is therefore 4 or 5.

The refined number of atoms (n) is reproducibly higher by about 0.7 in samples of SLO^N·MeOH and is consistent (by the same error analysis given earlier) with a true n of 5 or 6. Furthermore, the refined iron−nitrogen distance is about 0.04 Å longer for SLO^N·MeOH. The refined parameters for a sample of SLO^N in 20% glycerol are intermediate between the parameters obtained for SLO^N and SLO^N·MeOH.

Fits 1, 2, 4, and 5 of Table 4 employ a mixed nitrogen/oxygen coordination shell and should give a more accurate average bond length. Three Fe−N bonds are assumed (as indicated by crystallography). As with the $Fe(acac)_3$ data, the refined bond lengths decrease when Fe−N bonds are replaced by Fe−O bonds in the model.

Tables 3 and 4 show the averages of results from refinements on individual data sets; identical parameters are obtained by averaging the data and then refining. Figures 5 and 6 show the fits to the Fourier transforms and Fourier-filtered $k^3\chi$ of the averaged data sets. The Fourier-filtered fits appear to be very similar to the data, except above $k = 11$ Å^{-1}, but even there, the calculated spectra generally lie within the esd of the data.

The XANES analysis (*vide supra*) leaves open the possibility of an unusually short or long bond in SLO^N, in addition to five normal length coordination bonds. Multiple-shell fits to the EXAFS of SLO^N or SLO^N·MeOH with a single short Fe−O shell resulted in only marginal improvements to the fit, but in any event it did not produce refined bond lengths shorter than 2.05 Å (Table S6). Experience with oxo-bridged diferric compounds has shown that when a single Fe−O bond is at least 0.15 Å shorter than the other bonds, its presence is clearly shown by the EXAFS fitting (Scarrow et al., 1987), and indeed we have evidence for a single unusually short bond in SLO^A. Thus, we can confidently rule out the possibility of an unusually short bond in SLO^N.

The control multishell refinements with data from $[Fe^{II}(N\text{-MeIm})_6]^{2+}$ revealed a limitation of EXAFS for detecting long (>2.5 Å) Fe−O or Fe−N bonds. The back-transform limits we have used are $r' = 1.0-2.3$ Å, and since the peak in the Fourier transform is usually at r' = bond length − 0.5 Å (Figure 5), we expected to be able to detect bond lengths of up to about 2.8 Å, with minimal interference from outer sphere scatterers at >3 Å. We initially believed that the low gof of fit 3 for Table 4 (and others shown in Table

Table 5: Summary of Fits to First Sphere Fourier-Filtered EXAFS of Samples of SLO^A Prepared without and with Added Alcohol (Methanol, Ethanol, or Glycerol)[a]

	shell 1			shells 2 and 3				
ID	n	r (Å)	$\Delta\sigma^2$ (Å^2)	n	r (Å)	$\Delta\sigma^2$ (Å^2)	gof	BVS
				SLO^A without ROH				
1	5.3(4)N	2.014(6)	0.00479(9)				2.5(4)	
2	5.4(6)N	2.122(4)	0.0011(10)	1O	1.88(2)	0.0006(9)	1.2(4)	
3	3N/2O	2.107(5)	0.0013(3)	1O	1.881(8)	0.0001(8)	1.3(5)	2.92(4)
				SLO^A with ROH				
2	4.9(5)N	2.138(10)	0.0010(3)	1O	1.90(2)	0.0003(4)	0.8(2)	
3	3N/2O	2.119(6)	0.0024(11)	1O	1.886(10)	−0.0001(7)	0.9(1)	2.87(5)

[a] Values are averages from refinements on similar data sets. Shown in parentheses are the esds of the last reported digit, based on variations in the refined parameters between data sets. Additional details are found in Table S8.

S6) indicated a single, long Fe−N or Fe−O bond of about 2.5 Å in samples of SLO^N. However, even larger reductions in the gof were obtained for a similar fit (8) to the EXAFS of $[Fe^{II}(N\text{-MeIm})_6]^{2+}$, where no such interaction exists. Fit 9, to data simulated by FEFF 5.05, also showed an apparent long Fe−N bond that is absent from the crystal structure; this implies that the appearance of a 2.5 Å bond in our fits can arise from incomplete removal (by Fourier filtering) of the EXAFS from outer sphere scatterers in bound imidazole groups.

The 2.5 Å artifactual shell in the EXAFS fits would obscure a 2.5−2.7 Å Fe−N or Fe−O bond, particularly if there were large vibrational disorder as expected for a weak bond, and even longer bonds would be unresolvable from true second sphere (two bonds removed) Fe−X distances. Thus, first sphere EXAFS analysis cannot confirm or deny the presence of Fe−O or Fe−N bonds in the 2.5−3.0 Å range (specifically, it cannot detect or refute the possible presence of the >2.5 Å iron−carboxamide (Asn) bond observed in one of the crystal structures of SLO^N; *vide infra*).

Ferric Lipoxygenase (SLO^A). As expected from the similarity of the data, results from fitting the EXAFS of SLO^A were nearly identical for samples prepared at pH 6, 7, and 9 (Tables S5 and S7); average results from these refinements, using various coordination models, are shown in Table 5. For the five SLO^A samples, single-shell fits (fit type 1) gave $n = 5.3$ and $r_{Fe-N} = 2.10$ Å. Much better fits, with gof decreased by half, were obtained when a shell containing a single oxygen atom at 1.88 Å was added to a shell of five nitrogen atoms at 2.12 Å (fit type 2). We decided to model the short shell as oxygen because Fe−O bonds are generally shorter than Fe−N bonds.

The average of the five longer bonds decreases by less than 0.02 Å when the longer shell is modeled as three nitrogen and two oxygen scatterers at the same distance (fit type 3). We tried many other fits to the EXAFS of SLO^A in which the first coordination sphere was modeled by one, two, or three shells of oxygen and/or nitrogen scatterers (Tables S7 and S8). All of the best fits (gof ≈ 1) imply a single Fe−O bond of length ca. 1.88 Å, with five remaining bonds longer than 2.00 Å, averaging 2.11 or 2.12 Å. Models missing the short Fe−O bond give poor fits to the data above $k = 7$ Å^{-1} (Figure 6c), resulting in a gof at least twice as large as those for the best fits.

The apparent exceptions to these generalizations are the good fits obtained when we assumed four Fe−N scatterers at 2.14 Å and two Fe−O scatterers near 1.95 Å (Table S7). However, for these fits, the refined $\Delta\sigma^2$ for the oxygen shell is anomalously high (ca. 0.008 Å^2). If we assume that the vibrational disorder is the same as that in the model compounds at low temperature, then the large $\Delta\sigma^2$ reflects static differences between the two Fe−O bond lengths: $\sigma_{static} = [\Delta\sigma^2]^{0.5} \approx 0.09$ Å. This implies that the two Fe−O equilibrium bond lengths are ca. 1.87 and 2.03 Å. Thus, these fits also support the presence of a single ca. 1.88 Å Fe−O bond, with remaining bonds longer than 2.00 Å.

Table S8 shows the results from additional fits with a single, short Fe−O bond but overall five- or seven-coordination. These fits yield a roughly 30% higher gof compared to the corresponding fits shown in Table 5, indicating that overall six-coordination for SLO^A is most consistent with EXAFS analysis. This is also indicated by the refined n for the Fe−N shell in type 2 fits (which also have a single, short Fe−O bond): 5.4 ± 0.6 in the absence or 4.9 ± 0.5 in the presence of alcohols. As mentioned for SLO^N, the true value is likely between 30% lower and 5% higher than the refined value; thus, the true number of oxygen and nitrogen atoms in this shell is most likely 5, but possibly 4. With the inclusion of the short Fe−O bond, the coordination number is 6, or less likely 5, by the EXAFS analysis alone.

In contrast to the results from SLO^N samples, EXAFS analyses for SLO^A samples prepared with and without added alcohols gave overlapping ranges of refined parameters (Tables 5, S7, and S8).

BVS Calculations and Coordination Numbers. Bond valence sum theory can be used to confirm that bond lengths from EXAFS are consistent with assigned oxidation states and coordination numbers (Liu & Thorpe, 1993; Thorp, 1992). Brown and Altermatt (1985) proposed that the sum of bond valences (BV) for all of the bonds around a metal (the BVS) should be close to the oxidation number of the atom. The BV are calculated from the deviation of the bond length r from an empirically derived distance, r_o, at which the bond valence would be unity: $BV = \exp((r_o - r)/0.37$ Å). Values of r_o depend on the identity of the bonded atoms and on the oxidation state of the metal. On the basis of their Inorganic Crystal Structure Database, Brown and Altermatt determined some values of r_o, including those of Fe^{III}−O (1.759 Å), Fe^{II}−O (1.734 Å), and Fe^{II}−N (1.806 Å). Their formulae indicate that for a transition metal, r_o(M−N) will

Table 6: Evidence for or against Various Coordination Numbers in Various Forms of Soybean Lipoxygenase[a]

	coordination no.						
	4	4+1	5	5+1	6	6+1	7
			SLO^N				
XANES	–	○[b]	●	○[b]	–	–	–
n from EXAFS	●	●	●	●	–	–	–
r from EXAFS (BVS)	–	–	○[c]	●	○[c]	–	–
overall	–	–	●	●	–	–	–
			SLO^N·MeOH or SLO^A[d]				
XANES	–	–	–	–	●	●	●
n from EXAFS	–	–	●	●	●	●	–
r from EXAFS (BVS)	–	–	–	–	●	●	–
overall	–	–	–	–	●	○[e]	–

[a] ●, consistent; ○, possibly consistent; –, inconsistent. n+1 coordination indicates n bonds with lengths <2.5 Å and one long bond of >2.5 Å. [b] In the absence of crystal structures and XANES data of model compounds with long Fe^{2+}–X bonds, it is not possible to predict the 1s→3d peak area for 4+1 or 5+1 coordination numbers. [c] Whether or not BVS lies within the range observed for model compounds depends on the exact details of the refinement model (Table S6). [d] Although based on different data, conclusions regarding coordination number are the same for SLO^N·MeOH and SLO^A (with or without added alcohol). [e] Considered unlikely because of steric crowding.

be about 0.072 Å longer than r_o(M–O); thus, we have used 1.831 Å as r_o for Fe^{III}–N.[4]

We have tested the BVS formalism on a collection of single-crystal structures of iron coordination complexes, shown in Table S9. [In selecting model complexes for Table S9, we made use of the Cambridge Structural Database System (Allen et al., 1991).] For high-spin complexes with only O and/or N coordination, we find ranges of 1.95 < BVS < 2.24 for Fe^{2+} (19 high-spin compounds) and 2.84 < BVS < 3.25 for Fe^{3+} (41 high-spin compounds). Coordination numbers range from 4 to 7 in the model compounds included, but this does not systematically affect the BVS. We expect that accurate coordination models for iron coordination based on EXAFS will yield BVS values within the ranges found for the model complexes.

BVS values are shown for the refined EXAFS bond lengths in Tables 4, 5, S6, and S8. These values reinforce the conclusions from XANES analysis that SLO^N·MeOH and SLO^A must have iron coordination numbers of at least six, since the BVS values for five-coordinate fits (fit 5 in Table 4, for instance) are at least 0.20 less than the minimal BVSs observed for Fe^{2+} and Fe^{3+} compounds, respectively. For SLO^N, five-coordinate fit 1 of Table 4 gives a BVS within the model compound range. Six-coordination cannot be ruled out by BVS analysis: although fit 2 of Table 4 gives a BVS 0.07 higher than those observed for Fe^{2+} compounds, refining the Fe–O and Fe–N distances separately (Table S6) lowers the BVS slightly so that it is within the observed range.

DISCUSSION

Table 6 summarizes the evidence from X-ray spectroscopy regarding the coordination numbers of the iron centers in SLO^N and SLO^N·MeOH. Because of the results from crystallography (*vide infra*), we have given explicit consideration to the possibility that an unusually long (>2.5 Å) Fe–O bond might be present. As stated earlier, we are unable to confirm or deny the existence of such a bond by our EXAFS analysis. We denote the possibility that such a bond is present in addition to five shorter bonds as 5+1 coordination. Taken together, our results indicate either 5 or 5+1 coordination for SLO^N and 6 or 6+1 coordination for SLO^N·MeOH and SLO^A.

SLO^N: Comparison to Previous EXAFS/XANES Studies. The XANES spectra (Figure 2a) between 7100 and 7150 eV are very similar to those reported earlier for SLO^N and SLO^A, but our EXAFS spectra ($k^3\chi$ vs k; Figure 2b) appear to be quite different from the earlier spectra [compare to Figure 1 of Van der Heijdt et al. (1992)]. The discrepancy in the EXAFS is attributable to a difference in E_0, the ionization energy of the Fe 1s orbital, which is refined by the *EXCURV88* software (Gurman et al., 1986) used in previous studies. This changes k (eq 3) and, thus, the display of EXAFS data ($k^3\chi$ vs k). In earlier studies on lipoxygenase, the refined ΔE_0 was 16 ± 1 eV for SLO^N (Feiters et al., 1990) and 14 ± 1 eV for SLO^A (Van der Heijdt et al., 1992). This value is subtracted from a reference energy of ca. 7120 eV (Feiters et al., 1990) to give E_0. By assuming the reference energy was 7116 eV, and using the resulting E_0 (7100 or 7102 eV) with our data (Figure 2c), we obtain EXAFS spectra with similar shapes and the same k for extrema and zero crossings as were found in the earlier reported spectra (Van der Heijdt et al., 1992). We note that these values of E_0 are physically unrealistic for ionization energies, coming below even the 1s→3d pre-edge transition.

Our conclusion that the XANES of SLO^N is consistent with five-coordination differs from that of Feiters and coworkers (Feiters et al., 1990), who report the pre-edge feature of SLO^N to be small and indicative of six-coordination. Their XANES data (with and without dioxygen present) appear to be very similar to ours. Feiters et al. do not report any quantitation of A_{pre} values, nor did they use XANES spectra from ferrous model compounds to support the conclusion of six-coordination. The similarity noted (Van der Heijdt et al., 1992) between the size of the feature in SLO^N and SLO^A is deceptive because iron(III) compounds have larger pre-edge peaks given the same coordination numbers (Randall, 1993).

The bond lengths we obtain from our one- and two-shell fits to the EXAFS of SLO^N (Tables 3 and 4) are, on average, 0.04–0.07 Å longer than the distances found by Feiters et al. (1990): they reported two Fe–O bonds at 1.99 Å and four Fe–N bonds at 2.14 Å. Given the similarity of their EXAFS data to ours, the shorter bond lengths obtained by Feiters et al. are probably attributable to their practice of using *EXCURV88* to refine a global (i.e., the same for all shells) E_0 along with bond lengths. To test this hypothesis, we used *EXCURV88* to refine r and E_0 simultaneously using our data from $[Fe^{II}(N\text{-MeIm})_6](BF_4)_2$. The E_0 refined to 7098 eV, which is only 2 eV less than the value apparently used by Feiters et al. (Figure 2c). The refined r was 2.13 Å, which is significantly shorter than the 2.20–2.21 Å found by crystallography (Miller et al., 1989; Seel et al., 1980). High correlations between r and E_0 and the importance of the correct choice of shell-specific E_{0i} for the determination of r_i have been demonstrated previously (Scarrow et al., 1987; Teo et al., 1983). In the present study, we have demonstrated

[4] In results not shown here, we have calculated the BVS using a revised r_o from Liu and Thorp (1993). Although the BVSs for all Fe(II) compounds are ca. 0.2 less by this method than the BVS we report, the conclusions (based on comparisons of BVSs derived from EXAFS analyses to BVSs from model crystal structures) are unchanged.

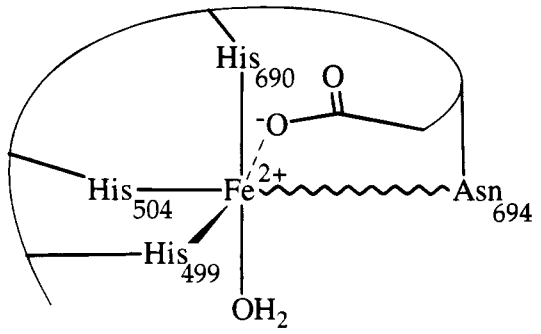

FIGURE 7: Structure of SLO^N from the crystallography of crystals of SLO^N grown at pH 5.6 (Minor et al., 1993; B. Axelrod, personal communication). The other published crystal structure lacks the Fe−Asn and Fe−H_2O bonds, and electron density maps suggest that these coordination positions are vacant (Boyington et al., 1993).

that the use of E_{0i} = 7125 eV with amplitude and phase functions from FEFF 5.05 gives refined values of r for simple model complexes that are generally within 0.01 Å of crystallographic values (Table 2), and so we have used this value in analyzing all Fe−O and Fe−N shells of protein samples.

SLO^N: Comparison to Results from Other Techniques. Both published crystal structures indicate coordination by three histidine residues and the C-terminal carboxylate ligand (Boyington et al., 1993; Minor et al., 1993). Boyington et al. (who obtained their crystals at pH 7.0) do not find additional liganding groups and they fail to detect appreciable electron density in difference maps of their 2.6 Å resolution structure, thus claiming a four-coordinate structure. The arrangement of the four ligands to iron is described by Boyington et al. as pseudo-octahedral, in which two *cis* coordination positions are assumed to be vacant on the basis of the distance of the closest amino acid side chains in the structure model and the lack of electron density in difference maps. However, at 2.6 Å resolution the evidence against coordinated water must be considered weak, and the geometry adopted by the four known ligands suggests to us that at least one and perhaps two waters are coordinated. The reported bond lengths in the Boyington structure average 2.18 Å, just 0.05 Å longer than our EXAFS-determined average bond length, which we consider to be good agreement considering the 2.6 Å resolution of the crystal structure.

Minor et al. grew their crystals at pH 5.6 and found a long bond between iron and a carboxamide atom (presumably O) of an asparagine residue. This research group is currently refining their structure to 1.4 Å resolution (B. Axelrod, personal communication) and now have evidence for a coordinated water. The arrangement of ligands is shown in Figure 7. The Fe−Asn distance in the higher resolution structure remains less than the van der Waals radii, but is roughly 0.5 Å longer than other bonds at the current stage of refinement. Thus, the Minor crystal structure shows 5+1 iron coordination and is consistent with our X-ray spectroscopic data for SLO^N (Table 6).

EXAFS at the current level of analysis cannot decide the question of whether the Fe−Asn bond is found in solution, but in conjunction with the crystal structures, it does strongly suggest that one (and only one) water is coordinated to the Fe^{2+} in SLO^N. Potentially, other spectroscopies could distinguish between five-coordination and 5+1 coordination for the iron in SLO^N. Previous studies of the CD, MCD (Whittaker & Solomon, 1986, 1988), and Mössbauer (Dunham et al., 1990) spectroscopic properties of SLO^N have concluded that the iron is six-coordinate; however, the MCD and Mössbauer results are equivocal.[5] The strongest evidence is in the room-temperature CD spectra, which show only a small splitting of the e_g orbitals of about 1500 cm^{-1}, consistent with a tetragonally distorted octahedral structure but not with five-coordination (Solomon & Zhang, 1992). From a ligand field standpoint, 5+1 coordination can be considered a perturbation of tetragonally elongated octahedral geometry in which one axial bond is compressed back to normal length and the other axial bond is lengthened; this anticentrosymmetric (u) distortion will have little effect on the energies of the centrosymmetric (g) d orbitals. Thus, we believe that both 6 and 5+1 coordination are compatible with the CD spectrum of SLO^N. Clearly, it is important to synthesize Fe(II) model compounds with 5+1 coordination to determine whether their spectroscopic properties match those of SLO^N.

Combining information from our XANES/EXAFS study with that from crystallography and CD spectroscopy, we suggest that the iron in SLO^N adopts the structure shown in Figure 7, in solution as well as in the crystal. This structure, with 5+1 coordination, is consistent with the spectroscopic results reported to date (including the present study) and has been found in one of the two types of SLO^N crystals investigated by crystallography. The X-ray and CD spectroscopic results are both inconsistent with the four-coordinate structure of the Boyington crystal structure.

SLO^A. For samples of active, Fe^{3+}-containing lipoxygenase (SLO^A), prepared either with or without small alcohols, analysis of the pre-edge peak area and the refined number of atoms and bond lengths from EXAFS allows the same conclusion about the coordination number of SLO^A that was reached for SLO^N·MeOH (Table 6), namely, that there are six-coordination bonds. The possibility that there is an additional very long Fe−O bond is considered unlikely because of the steric crowding this would entail. The more likely possibility, that the iron is in a distorted octahedral environment, is in agreement with previous XANES and MCD studies.

Application of a two-shell model for the first coordination sphere substantially improved the fit to the EXAFS data. The best fits were obtained with a model of five bonds of 2.11−2.12 Å and one bond of 1.87−1.89 Å. These distances are virtually the same as those reported from a previous EXAFS study of SLO^A, but the previous study found three imidazole ligands at the longer 2.11 Å distance and three oxygen ligands at the shorter 1.90 Å distance (Van der Heijdt et al., 1992). Our EXAFS fits give no evidence for more than one Fe−O bond with r < 2.00 Å; as we increase the number of Fe−O bonds in the short shell, the refined r increases. Furthermore, the bond lengths reported by Van

[5] The MCD data that support octahedral coordination were obtained using frozen samples prepared in buffer containing 50% glycerol as a glassing agent (Whittaker & Solomon, 1986, 1988); since we have shown that glycerol induces coordination changes, the MCD results may not apply to the structure of SLO^N without alcohol present. The Mössbauer spectrum for frozen solutions of SLO^N shows a large ΔE_q = 3.08 mm/s, which was interpreted as indicating a distorted octahedral site for the ferrous ion (Dunham et al., 1990); however, metapyrocatechase contains a high-spin ferrous ion that is five-coordinate, based on its near-IR CD spectrum (Mabrouk et al., 1991), and shows ΔE_q = 3.28 mm/s (Tatsuno et al., 1980).

der Heijdt et al. result in a calculated BVS = 3.41, which is considerably higher than the highest value (3.25) we have found for high-spin ferric model complexes. Thus, we believe that the earlier analysis of the EXAFS for SLO^A is inaccurate, probably due to the use of a refined E_0, rather than one based on models, as discussed earlier for SLO^N.

The short bond is too short to be Fe−N even if one of the coordinated imidazole groups were to deprotonate. For instance, in the low-spin complex bis(4-methylimidazolato)-(tetraphenylporphinato)iron(III) (Quinn et al., 1983), the bonds between the iron and the deprotonated imidazolate ligands are 1.93 and 1.96 Å. On the basis of comparisons of ionic radii (Shannon, 1976), the Fe−N(imidazolate) bonds would be about 0.1 Å longer if the iron were high-spin, as it is in SLO^A. Thus, the ca. 1.88 Å distance must be an Fe−O bond length. This bond is much shorter than that found for coordinated carboxylate or water ligands, but it is in the range commonly found for aryloxy ligands bound to high-spin Fe^{3+}; 15 examples of high-spin Fe^{3+} complexes with Fe−OR (R = aryl) bonds of 1.86−1.93 Å are found in Table S9. However, such ligands bound to Fe^{3+} give rise to fairly intense ($\epsilon > 1000\ M^{-1}\ cm^{-1}$) ligand to metal charge transfer bands in the visible spectrum, which are absent for lipoxygenase. Thus, the short Fe−O bond arises from either an alkoxy or a hydroxy ligand, which both give similarly short Fe−O bonds in mononuclear complexes. Examples are the two nonbridging Fe^{3+}−alkoxy bonds of 1.91 and 1.92 Å in Fe^{III}(TIEO)(TIEOH) (Gorun et al., 1987) and the 1.91 Å Fe^{3+}−OH^- bonds found in two recently reported $[L(H_2O)Fe^{III}OFe^{III}(OH)L]^{3+}$ structures (L = tris(2-pyridylmethyl)amine or its 5-ethyl derivative) (Hazell et al., 1994; Wilkinson et al., 1994). Since no serine or threonine group is adjacent to the active site in the crystal structure, the short Fe−O bond can only reasonably be ascribed to a hydroxide ligand to Fe^{3+}. The 1.88 Å Fe−O bond length in SLO^A is slightly shorter than that found in the model structures; the difference may be due to the absence, in SLO^A, of a strong hydrogen bond to the OH^-, as found in the models. The presence of an $[Fe^{III}OH]^{2+}$ unit is consistent with the prediction of a ligand derived from water based on EPR line-broadening experiments (Nelson, 1988b).

If we assume that the three Fe−His and one Fe−carboxylate bonds seen in SLO^N remain in SLO^A, there must be one additional bond in the 2.0−2.3 Å range to fulfill six-coordination. The EPR line-broadening experiments would be consistent with the presence of a water ligand in addition to the bound hydroxide; other possibilities are bidentate coordination by the carboxylate or a ca. 0.5 Å shortening of the Fe−Asn bond relative to its length in SLO^N.

The EXAFS and XANES analyses indicate no change in the coordination of SLO^A over the pH range 5.8−9.0. Thus, if the $[Fe^{III}OH]^{2+}$ protonates to form $[Fe^{III}OH_2]^{3+}$, it does so only at pH 5 or less. This is not suprising; the pK_{a1} and pK_{a2} of $[Fe(H_2O)_6]^{3+}$ are both less than 3 (Martell & Smith, 1989), and the pK_a of water coordinated to the iron(III) complex of *N*-(2-aminoethyl)iminodiacetic acid is 3.9 (Anderegg & Schwarzenbach, 1955; Martell & Smith, 1974).

Effects of Alcohols on SLO^N and SLO^A. The iron K-edge X-ray spectra of SLO^N were found to be the same for samples prepared at pH 7 and 9, but they revealed a change in the coordination of the Fe^{2+} in the presence of low levels (0.1%, 20 mM) of methanol. This unexpected finding was the fortuitous result of a control experiment for our study of SLO^A reduced by the addition of linoleic acid in methanol (*vide infra*). The phenomenon we observe with methanol apparently is saturable within the low millimolar range: the relatively small change in the pre-edge transition and EXAFS-derived bond lengths observed upon going from 0.1% methanol to 1% methanol suggests that the coordination change is virtually complete in 0.1% (20 mM) methanol. Glycerol induces a similar change. More work will be needed to establish whether other alcohols cause a similar change in the iron coordination in SLO^N.

Excluding any possible long (>2.5 Å) Fe−O or Fe−N bond, our XANES and EXAFS analyses indicate that the number of bonds increases from five to six when methanol is added to SLO^N (Table 6). A likely explanation for the shift to 6-coordination in SLO^N·MeOH is that methanol forms a coordinate bond to the iron. The data would also be consistent with methanol binding elsewhere near the active site, causing a conformational change that allows a second water molecule to bind to the iron. Conformational changes could also allow the terminal carboxylate to bind in a bidentate fashion or the Fe−Asn bond to shorten to 2.3 Å or less. Synthetic iron(II) complexes crystallized from DMF show bonds in this range between Fe(II) and the oxygen atom of DMF (Gerli et al., 1991; Reiff et al., 1983b; Stremple et al., 1981).

Although this report is, to our knowledge, the first demonstration of an effect of alcohol on SLO^N, small alcohols have previously been reported to affect the physical properties of SLO^A. The addition of millimolar concentrations of any of several small alcohols eliminates the substantial microheterogeneity in the iron site seen in the EPR spectra of frozen samples of both SLO^A (Slappendel et al., 1982b) and the NO complex of SLO^N (Nelson, 1987). In both cases, the alcohol effect is a saturable phenomenon, with an effective K_D in the 1−10 mM range. Higher concentrations (15%) of glycerol also reduce the microheterogeneity of the EPR signal for SLO^A (Gaffney et al., 1993). Our XANES spectra show no significant effect of the alcohols added to SLO^A, and the EXAFS analysis reveals no clear differences. Thus, the iron undergoes only a relatively minor coordination change coincident with the sharpening of the EPR signal, which is consistent with evidence from NMR relaxation measurements that suggests that the alcohol does not coordinate the iron in SLO^A, but does bind to the enzyme in the vicinity of the active site (Slappendel et al., 1982a).

Substrate-Reduced Lipoxygenase (SLO^R). Mechanism A of Figure 1 implies that it should be possible to stop after step A1 by reacting SLO^A with linoleic acid under anaerobic conditions. Under these conditions, it has been shown that the iron is reduced and the products formed likely derive from an organic radical intermediate (de Groot et al., 1973; Garssen et al., 1972; Van der Heijdt et al., 1993). To account for the observed stereospecificity of the normal lipoxygenase reaction, the dissociation rate of the linoleate radicals from the reduced SLO must be much slower than the rate of step A2 (under 0.2 atm of O_2). Thus, by mixing SLO^A with linoleic acid until the yellow color of the ferric center in SLO^A disappeared (about 1 min at 4 °C) and then freezing the sample, we hoped to generate a sample of SLO with reduced iron and substantial amounts of linoleate radical bound to the enzyme. We denote the form of the enzyme prepared by this technique as SLO^R. A similar procedure

has been used to prepare samples for Mössbauer spectroscopy. The Mössbauer spectrum of of SLO^R was reported to have high-spin iron(II) in a coordination environment distinctly different from that of SLO^N (Funk et al., 1990). Thus, we looked for evidence, using X-ray spectroscopy, of differences in iron coordination between SLO^R and SLO^N.

We began by investigating the reduction of SLO^A by a nonphysiological reductant, pyrocatechol (Nelson, 1988a). Upon mixing the concentrated solutions of protein and reductant, there was rapid and complete loss of the yellow color, and the sample frozen after ca. 30 s (3D7c) had XANES and EXAFS properties indistinguishable from those of samples of SLO^N (Tables 3 and S3). Our attempts to reduce concentrated samples of SLO^A with linoleic acid suspended in borate buffer resulted in very slow and only partial disappearance of the yellow color of the ferric enzyme; the X-ray spectra of the sample frozen after 1 min suggested incomplete reduction of the iron at the time of freezing. To aid in the mixing of concentrated solutions of protein and linoleic acid, we adopted the procedure used in the Mössbauer study and anaerobically treated samples of SLO^A with excess linoleic acid, added as a methanol solution (final concentration of methanol was approximately 0.1%). The resulting spectra, while distinct from those of SLO^N, are very similar to those of SLO^N·MeOH; small differences in the spectra and refined parameters can be attributed to the presence of a small percentage of unreduced SLO^A.

Thus, XANES and EXAFS give no evidence that the reduction of SLO^A by either linoleic acid or pyrocatechol yields a ferrous site different from that in SLO^N, although the presence of methanol in the linoleic acid reductant solution does cause a significant change. Our results suggest that the coordination change observed by Mössbauer spectroscopy and attributed to the effects of reduction by substrate simply may have resulted from the addition of methanol to SLO^N. The change in Mössbauer parameters observed (ΔE_q-(SLO^N), 3.08 mm/s; $\Delta E_q(SLO^R)$, 2.54 mm/s) is consistent with a shift to a more centrosymmetric environment, in line with our conclusion concerning the effect of methanol on the ferrous ion. Recognizing that Mössbauer spectroscopy is much more sensitive to changes in coordination than is XANES, we conclude that a difference in structure between the ferrous ion in SLO^N and that in substrate-reduced SLO^A (SLO^R) remains to be demonstrated.

Implications for the Mechanism. Our data indicate that SLO^N has only five normal length coordination bonds, but that the iron(II) is capable of forming a sixth such bond upon the addition of methanol or glycerol. This flexibility in coordination number raises the possibility that either oxygen or a fatty acid intermediate might coordinate the iron at an intermediate state in the catalysis (perhaps in step A2 of Figure 1). Coordination of dioxygen could activate the O_2 toward reaction with the fatty acid intermediate and direct the approach of oxygen to the 13-*pro-S* position (Nelson et al., 1994). The affinity of SLO^N for dioxygen must be very low: no measurable effect of oxygen on the physical properties of the enzyme has been reported (Feiters et al., 1985, 1990; Petersson et al., 1985). On the other hand, the ferrous ion in the catalytic intermediate may have substantially higher oxygen affinity than that in SLO^N. In any event, a thermodynamically unstable ferrous−dioxygen complex might still be kinetically competent to be a mechanistic intermediate.

One unanswered mechanistic question has been the identity of the basic residue (B:) that stereospecifically removes a proton from C-11 of linoleic acid in step A1 or B1 of the alternate mechanisms of Figure 1. The details of this step are particularly important because of the unusually large primary kinetic isotope effect associated with the enzymatic reaction; independent groups have measured $^D(V/K)$ values of 30−50 using [11,11-$^2H_2$]linoleic acid as a substrate for SLO^A (Glickman et al., 1994; Hwang & Grissom, 1994). The crystal structures have revealed no obvious candidates for the proton acceptor from the protein residues; Boyington et al. (1993) suggested that a histidine residue may dissociate from the iron in order to act as the base or that the non-coordinated oxygen of the C-terminal carboxylate may play this role. The former suggestion is plausible, but the latter suffers from the low basicity expected for a carboxylate coordinated to a positively charged metal ion.

In this paper, we have presented evidence for a hydroxide ligand bound to Fe^{3+} in SLO^A. We believe that the $[Fe^{III}OH]^{2+}$ unit in SLO^A is an excellent candidate for the active-site base. Although not particularly basic ($pK_a < 5.5$), it may function as an electron acceptor as well as a proton acceptor. Thus, step A1 of Figure 1 could occur by H-atom transfer to the $[Fe^{III}OH]^{2+}$, yielding $[Fe^{II}OH_2]^{2+}$ and giving rise to the water ligand seen in the structure of SLO^N (Figure 7). This step would leave the iron six-coordinate. Since SLO^N is 5 or 5+1 coordinate, it is plausible that the next step of the mechanism would be the dissociation of a ligand (water, one oxygen of a bidentate carboxylate, or a short Fe−Asn bond) to give either the structure in Figure 7 or a true five-coordinate Fe^{2+} form (lacking the long Fe−Asn bond). In either case, the iron would be coordinatively unsaturated, which would favor the rapid binding and activation of O_2.

Recent observation by EPR of enzyme-bound radicals attributable to intermediates or side products of pathway A in Figure 1 (Chamulitrat & Mason, 1989; Nelson & Cowling, 1990; Nelson et al., 1990, 1994) provides strong support for that mechanism. However, we note that the hydroxide ligand could also act as a base for the first step of the organometallic mechanism (step B1). In this case, the driving force would be provided by a concerted proton transfer and the formation of an Fe−C bond proceeding through a 6-membered cyclic transition state. This proposal would require the reversable loss of one of the non-hydroxide ligands of SLO^A prior to the rate-limiting concerted formation of the organometallic intermediate.

Finally, we describe an interesting possibility suggested by recent studies of the reactions of synthetic complexes containing $[Fe^{II}OH_2]^{2+}$ units with radicals. It has been shown, for example, that $[LFe^{II}(OH)_2]^-$ (where L is nitrilotriacetato) reacts with methyl radical to yield $[LFe^{III}(CH_3)]^-$, with a first-order rate constant of 10^7 M^{-1} s^{-1} (Van Eldik et al., 1994). This suggests that the species generated by step A1 in Figure 1, which we are postulating is a noncovalent complex between $[Fe^{II}OH_2]^{2+}$ enzyme and a substrate radical, would rapidly convert by step C to an organoiron(III) complex and then follow path B to product. This would neatly rationalize how the enzyme can utilize a radical mechanism to generate 13(*S*)-HPOD regioselectively and stereospecifically.

Summary. The XANES and EXAFS spectra of SLO^N and SLO^A have been analyzed with the following results: (1)

SLO^N in frozen solutions contains a ferrous ion with five Fe−O and Fe−N bonds close to and averaging 2.13 ± 0.01 Å in length. The possibility of a sixth bond of length greater than 2.5 Å cannot be excluded. These and other spectroscopic measurements for solutions of SLO^N are consistent with the crystal structure (Figure 7) of Minor and co-workers (Minor et al., 1993; B. Axelrod, personal communication). (2) The addition of methanol or glycerol increases the number of bonds <2.5 Å to six and lengthens the average metal−ligand bond length by 0.04 Å. The binding of methanol to SLO^N is virtually complete at 20 mM. The coordination number increase is consistent with, but does not imply, direct coordination of the methanol to the ferrous ion. (3) SLO^A in frozen solutions also has six bonds, excluding a possible long bond of >2.5 Å. One of these bonds has a length of 1.88 ± 0.02 Å, indicating a hydroxide ligand, and the other five are close to and average 2.11 ± 0.01 Å in length. (4) We have not obtained evidence for any substrate- or oxygen-bound intermediates and suggest that previous reports of substrate-bound iron(II) intermediates should be re-examined for the possibility that they reflect the formation of small alcohol adducts of SLO^N.

ACKNOWLEDGMENT

We thank Gerry Lamble, Simon George, and Syed Khalid at the NSLS for guidance; Hai-Yong Jin, Joyce Whitehead, Henriette Kuehne, and Bridget Brennan for assistance in data collection; Lawrence Que, Jr., Steven Cramer, and Britton Chance for the use of equipment; Dr. Ninian Blackburn for computer time and guidance in the use of *EXCURV88*; Clay Randall and L. Que, Jr., for prepublication use of their XANES data; and Saqib Rehman for assistance in preparing Table S9.

SUPPLEMENTARY MATERIAL AVAILABLE

Tables describing the calculation of $F_{rel}(E)\mu_{rel}^{FeK}(E)$ used in eq 1 (Table S1), f and α functions used in calculations (Table S2), values of A_{pre} for Fe^{2+} (Table S3) and Fe^{3+} (Table S4) forms of SLO and model complexes, single-shell fits to individual data sets (Table S5), alternative one- and two-shell fits to EXAFS of SLO^N, SLO_N·MeOH, and $[Fe(N\text{-}MeIm)_6]^{2+}$ (Table S6), two-shell fits to individual SLO^A data sets (Table S7), alternative one-, two-, and three-shell fits to SLO^A and SLO^A+alcohol (Table S8), and bond lengths and BVS calculations for crystallographically characterized high-spin iron(II) and iron(III) compounds (Table S9) (13 pages). Ordering information is given on any current masthead page.

REFERENCES

Allen, F. H., Davies, J. E., Galloy, J. J., Johnson, O., Kennard, O., Macrae, C. F., Mitchell, E. M., Mitchell, G. F., Smith, J. M., & Watson, D. G. (1991) *J. Chem. Inf. Comput. Sci. 31*, 187−204.

Anderegg, G., & Schwarzenbach, G. (1955) *Helv. Chim. Acta 38*, 1940−1942.

Armstrong, W. H., Spool, A., Papaefthymiou, G. C., Frankel, R. B., & Lippard, S. J. (1984) *J. Am. Chem. Soc. 106*, 3653−3667.

Boyington, J. C., Gaffney, B. J., & Amzel, L. M. (1993) *Science (Washington D.C.) 260*, 1482−1486.

Brown, I. D., & Altermatt, D. (1985) *Acta Crystallogr., Sect. B 41*, 244−247.

Chamulitrat, W., & Mason, R. P. (1989) *J. Biol. Chem. 264*, 20968−20973.

Cheesbrough, T. M., & Axelrod, B. (1983) *Biochemistry 22*, 3837−3840.

Cingi, M. B., Lanfredi, A. M. M., Tiripicchio, A., Cornelissen, J. P., Haasnoot, J. G., & Reedijk, J. (1986) *Acta Crystallogr., Sect. C: Cryst. Struct. Commun. C42*, 1296−1298.

Corey, E. J., & Nagata, R. (1987) *J. Am. Chem. Soc. 109*, 8107−8108.

Cox, D. D., & Que, L., Jr. (1988) *J. Am. Chem. Soc. 110*, 8085−8092.

Cox, D. D., Ballinger, T. A., Benkovic, S. J., Bloom, L. M., Bradley, F. C., Nelson, M. J., Que, L., Jr., & Wallick, D. E. (1988) *J. Am. Chem. Soc. 110*, 2026−2032.

de Groot, J. J. M. C., Garssen, G. J., Vliegenthart, J. F. G., & Boldingh, J. (1973) *Biochim. Biophys. Acta 326*, 279−284.

de Groot, J. J. M. C., Veldink, G. A., Vliegenthart, J. F. G., Boldingh, J., Wever, R., & Van Gelder, B. F. (1975) *Biochim. Biophys. Acta 377*, 71−79.

Dunham, W. R., Carroll, R. T., Thompson, J. F., Sands, R. H., & Funk, M. O. (1990) *Eur. J. Biochem. 190*, 611−617.

Feiters, M. C., Aasa, R., Malmström, B. G., Slappendel, S., Veldink, G. A., & Vliegenthart, J. F. G. (1985) *Biochim. Biophys. Acta 831*, 302−305.

Feiters, M. C., Boelens, H., Veldink, G. A., Vliegenthart, J. F. G., Navaratnam, S., Allen, J. C., Nolting, H. F., & Hermes, C. (1990) *Recl. Trav. Chim. Pays Bas 109*, 133−146.

Funk, M. O., Carroll, R. T., Thompson, J. F., Sands, R. H., & Dunham, W. R. (1990) *J. Am. Chem. Soc. 112*, 5375−5376.

Gaffney, B. J., Mavrophilipos, D. V., & Doctor, K. S. (1993) *Biophys. J. 64*, 773−783.

Gardner, H. W. (1991) *Biochim. Biophys. Acta 1084*, 221−239.

Garssen, G. J., Vliegenthart, J. F. G., & Boldingh, J. (1972) *Biochem. J. 130*, 435−442.

Gerli, A., Hagen, K. S., & Marzilli, L. G. (1991) *Inorg. Chem. 30*, 4673−4676.

Glickman, M. H., Wiseman, J. S., & Klinman, J. P. (1994) *J. Am. Chem. Soc. 116*, 793−794.

Gorun, S. M., Papaefthymiou, G. C., Frankel, R. B., & Lippard, S. J. (1987) *J. Am. Chem. Soc. 109*, 4244−4255.

Gurman, S. J., Binsted, N., & Ross, I. (1986) *J. Phys. C: Solid State Phys. 19*, 1845−1861.

Hazell, A., Jensen, K. B., McKenzie, C. J., & Toftlund, H. (1994) *Inorg. Chem. 33*, 3127−3134.

Hwang, C.-C., & Grissom, C. B. (1994) *J. Am. Chem. Soc. 116*, 795−796.

Iball, J., & Morgan, C. H. (1967) *Acta Crystallogr. 23*, 239−244.

Kitajima, N., Fukui, H., Morooka, Y., Mizutani, Y., & Kitagawa, T. (1990) *J. Am. Chem. Soc. 112*, 6402−6403.

Liu, W., & Thorpe, H. H. (1993) *Inorg. Chem. 32*, 4102−4105.

Mabrouk, P. A., Orville, A. M., Lipscomb, J. D., & Solomon, E. I. (1991) *J. Am. Chem. Soc. 113*, 4053−4061.

Martell, A. E., & Smith, R. M. (1974) *Critical Stability Constants*, Vol. 1, Plenum, New York.

Martell, A. E., & Smith, R. M. (1989) *Critical Stability Constants*, Vol. 6, Plenum, New York.

McDevitt, M. R., Addison, A. W., Sinn, E., & Thompson, L. K. (1990) *Inorg. Chem. 29*, 3425−3433.

McKale, A. G., Veal, B. W., Paulikas, A. P., Chan, S.-K., & Knapp, G. S. (1988) *J. Am. Chem. Soc. 110*, 3763−3768.

McMaster, W. H., Kerr Del Grande, N., Mallett, J. H., & Hubbell, J. H. (1969) *Compilation of X-ray Cross Sections*, Vol. UCRL-50174 Sec. II, Rev. 1, National Technical Information Service, U.S. Chamber of Commerce, Springfield, VA.

Miller, L. L., Jacobson, R. A., Chen, Y. S., & Kurtz, D. M., Jr. (1989) *Acta Crystallogr., Sect. C: Cryst. Struct. Commun. C45*, 527−529.

Minor, W., Steczko, J., Bolin, J. T., Otwinowski, Z., & Axelrod, B. (1993) *Biochemistry 32*, 6320−6323.

Navaratnam, S., Feiters, M. C., Al-Hakim, M., Allen, J. C., Veldink, G. A., & Vliegenthart, J. F. G. (1988) *Biochim. Biophys. Acta 956*, 70−76.

Nelson, M. J. (1987) *J. Biol. Chem. 262*, 12137−12142.

Nelson, M. J. (1988a) *Biochemistry 27*, 4273−4278.

Nelson, M. J. (1988b) *J. Am. Chem. Soc. 110*, 2985−2986.

Nelson, M. J., & Cowling, R. A. (1990) *J. Am. Chem. Soc. 112*, 2820−2821.

Nelson, M. J., Cowling, R. A., & Seitz, S. P. (1990) *Biochemistry 29*, 6897−6903.

Nelson, M. J., Cowling, R. A., & Steitz, S. P. (1994) *Biochemistry 33*, 4966−4973.

Petersson, L., Slappendel, S., & Vliegenthart, J. F. G. (1985) *Biochim. Biophys. Acta 828*, 81−85.

Quinn, R., Strouse, C. E., & Valentine, J. S. (1983) *Inorg. Chem. 22*, 3934−3940.

Randall, C. R. (1993) Ph.D. Thesis, University of Minnesota, Minneapolis, MN.

Rehr, J. J., de Leon, J. M., Zabinsky, S. I., & Albers, R. C. (1991) *J. Am. Chem. Soc. 113*, 5135−5140.

Rehr, J. J., Albers, R. C., & Zabinsky, S. I. (1992) *Phys. Rev. Lett. 69*, 3397−3400.

Reiff, W. M., Witten, E. H., Mottle, K., Brennan, T. F., & Garafalo, A. R. (1983a) *Inorg. Chim. Acta 77*, L83−L88.

Reiff, W. M., Witten, E. H., Mottle, K., Brennan, T. F., & Garafalo, A. R. (1983b) *Inorg. Chim. Acta 77*, L27−L30.

Roe, A. L., Schneider, D. J., Mayer, R. J., Pyrz, J. W., Widom, J., & Que, L., Jr. (1984) *J. Am. Chem. Soc. 106*, 1676−1681.

Sayers, D. E., & Bunker, B. A. (1988) in *X-ray Absorption: Principles, Applications, Technique of EXAFS, SEXAFS and XANES* (Koningsberger, D. C., & Prins, R., Eds.) pp 211−253, Wiley, New York.

Scarrow, R. C., Maroney, M. J., Palmer, S. M., Que, L., Jr., Roe, A. L., Salowe, S. P., & Stubbe, J. (1987) *J. Am. Chem. Soc. 109*, 7857−7864.

Scott, R. A. (1985) *Methods Enzymol. 117*, 414−459.

Seel, F., Lehnert, R., Bill, E., & Trautwein, A. (1980) *Z. Naturforsch., B: Anorg. Chem., Org. Chem. 35b* (5), 631−638.

Shannon, R. D. (1976) *Acta Crystallogr., Sect. A A32*, 751−67.

Siedow, J. N. (1991) *Annu. Rev. Plant Physiol. Plant Mol. Biol. 42*, 145−188.

Slappendel, S., Aasa, R., Falk, K. E., Malmström, B. G., Vänngård, T., Veldink, G. A., & Vliegenthart, J. F. G. (1982a) *Biochim. Biophys. Acta 271*, 266−271.

Slappendel, S., Aasa, R., Malmström, B. G., Verhagen, J., Veldink, G. A., & Vliegenthart, J. F. G. (1982b) *Biochim. Biophys. Acta 708*, 259−265.

Slappendel, S., Malmström, B. G., Petersson, L., Ehrenberg, A., Veldink, G. A., & Vliegenthart, J. F. G. (1982c) *Biochem. Biophys. Res. Commun. 108*, 673−677.

Solomon, E. I., & Zhang, Y. (1992) *Acc. Chem. Res. 25*, 343−352.

Stremple, P., Baenzinger, N. C., & Coucouvanis, D. (1981) *J. Am. Chem. Soc. 103*, 4601−4603.

Tatsuno, Y., Saeki, Y., Nozaki, M., Otsuka, S., & Maeda, Y. (1980) *FEBS Lett. 112*, 83−86.

Teo, B. K., & Lee, P. A. (1979) *J. Am. Chem. Soc. 101*, 2815−2832.

Teo, B. K., Antonio, M. R., & Averill, B. A. (1983) *J. Am. Chem. Soc. 105*, 3751−3762.

Thorp, H. H. (1992) *Inorg. Chem. 31*, 1585−1588.

Van der Heijdt, L. M., Feiters, M. C., Navaratnam, S., Nolting, H. F., Hermes, C., Veldink, G. A., & Vliegenthart, J. F. G. (1992) *Eur. J. Biochem. 207*, 793−802.

Van der Heijdt, L. M., van der Lecq, F., Lachmansingh, A., Versluis, K., van der Kerk-van Hoof, A., Veldink, G. A., & Vliegenthart, J. F. G. (1993) *Lipids 28*, 779−782.

van Eldik, R., Cohen, H., & Meyerstein, D. (1994) *Inorg. Chem. 33*, 1566−1568.

Whittaker, J. W., & Solomon, E. I. (1986) *J. Am. Chem. Soc. 108*, 835−836.

Whittaker, J. W., & Solomon, E. I. (1988) *J. Am. Chem. Soc. 110*, 5329−5339.

Wilkinson, E. C., Dong, Y., & Que, L., Jr. (1994) *J. Am. Chem. Soc. 116*, 8394−8395.

Zalkin, A., Templeton, D. H., & Ueki, T. (1973) *Inorg. Chem. 12*, 1641−1646.

Zhang, Y., Gebhard, M. S., & Solomon, E. I. (1991) *J. Am. Chem. Soc. 113*, 5162−5175.